Hindawi
Advances in Materials Science and Engineering
Volume 2022, Article ID 1843131, 8 pages
https://doi.org/10.1155/2022/1843131

Research Article

The Shear Damage Model of the Two-Component Forming Polymer Grouting Material-Bentonite Contact Surface

Hao Zhang,[1] **Mingrui Du**,[2] **Yan Zhao**,[3] **and Liangqiong Chen**[1]

[1]*School of Architecture and Civil Engineering, Xinyang Normal University, Xinyang 464000, China*
[2]*School of Water Conservancy Engineering, Zhengzhou University, Zhengzhou 450001, China*
[3]*Harbin Institute of Technology National Engineering Research Center of Water Resources Co. LTD, Harbin 150000, China*

Correspondence should be addressed to Mingrui Du; dumingruicumt@sina.com

Received 9 October 2021; Accepted 14 March 2022; Published 21 April 2022

Academic Editor: Xin Cai

The newly developed two-component polymer (TFPU) cut-off walls have great application potential in civil engineering for water-seepage prevention. Investigating the mechanical interactions between TFPU and soil from the theoretical perspective can provide a basis for furtherly evaluating the stability of TFPU cut-off walls, which, however, has not been conducted. In this study, based on the shear testing results, the shear damage model of the TFPU-bentonite contact surface was established. Studies show that the TFPU-bentonite contact surface performs strain-softening behavior under shear and that the strain-softening behavior becomes less and less obvious when the normal stress increases. The theoretical shear stress-strain curves are in good consistent with the experimental ones, and the maximum differences between the theoretical shear stress and shear strain at yield and the experimental ones are about 3.88% and 3.40%, respectively, indicating that the shear damage model can reflect the mechanical properties of the TFPU-bentonite contact surface. The critical damage of the contact surface increases from 0.05 to 0.50 in the power function way when normal stress increases from 75 to 1200 kPa, implying that the shear failure of the contact surfaces changes from brittleness to ductility. This study provides a theoretical base for evaluating the influences of the TFPU-soil contact surface on the stability of the TFPU cut-off wall structures.

1. Introduction

In geotechnical engineering, water seepage has become the main cause of the various engineering accidents [1–5]. The cut-off walls are the most commonly adopted antiseepage measurement [6–8]. The polymer cut-off wall technique is a newly proposed method that uses the two-component foaming polyurethane as an alternative to the traditional concretes to construct cut-off walls [9–11]. As shown in Figure 1, the two-component polymer (TFPU) cut-off wall is built in the soil using the grouting technology [9, 10]. By virtue of the features of light-weight, low-stiffness, fast-construction, easy construction, good durability, strong permeability resistance, and environmental protection [12, 13], TFPU cut-off walls have found their applications in enhancing the permeability resistance of soil dams [9, 14, 15] and underground ancient grave [16]. Moreover, TFPU cut-off walls also hold a great application potential in the landfills and underground storage where seepage prevention is required [9, 15, 17, 18].

In actual engineering, except for playing the role of water barriers, the constructed TFPU cut-off walls sustain the external load [9]. Previous studies on the mechanical behaviors of TFPU cut-off walls used in soil dams have claimed that, under the action of the horizontal hydrostatic pressure, the TFPU cut-off walls will deform along with the deformation of the soil masses [19–21]. Studies have claimed that the deformation of the TFPU cut-off walls is mainly the flexural and stretching deformation [19, 20]. TFPU belongs to the category of high polymer, and its strength is mainly due to the entanglement between adjacent molecular chains [12, 13], but soil is a collection of solid particles, between which the Van der Waals force contributes to the cohesion strength [22]. The mechanical properties of TFPU are often

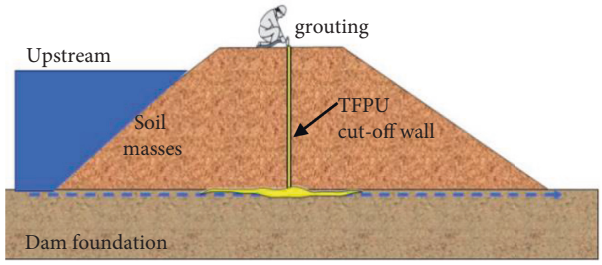

Figure 1: Schematic diagram of the construction of the two-component foaming polymer (TFPU) cut-off wall in soil dams [9].

different from the soil [13, 22–24]. Considering that TFPU cut-off walls are directly contacting with the soil, the bending and stretching deformation of TFPU cut-off walls will lead to the slip failure of the contact surface [11, 19, 25]. With the development of the TFPU cut-off wall technique, the contact surface between the TFPU matrices and soil becomes more and more in civil engineering. The investigation on the mechanical interactions of the TFPU-soil contact surface is of great engineering significance [9]. In our previous study [26], the shear strength of the TFPU-bentonite contact surface has been experimentally measured. The study was focused on the effects of the moisture content of bentonite and the density of TFPU on the shear strength of the TFPU-bentonite contact surface. Establishing a mechanical model that can reflect the shearing mechanical behavior of the TFPU-bentonite contact surface can provide a base for the further revealing of the mechanism of the coordination deformation between the cut-off wall structures and soil [20, 27–29], which, however, has not been carried out yet.

The damage mechanics theory has been widely used to describe the mechanical laws of heterogeneous materials such as concrete [30, 31], rock [32–34], soil [35], and polymers [13] in the failure process under external load. It has been proved that the theoretical models established based on the damage mechanics theory can also reflect the strength and deformation characteristics of the soil-rock or soil-concrete contact surfaces under shear [28, 29, 36]. Here, the primary experimental procedure and results of our previously work on the shear strength of the TFPU-bentonite contact surface are presented. Then, based on the experimental results, by combining the damage mechanics theory and the Weibull damage statistical equation, the shear damage model of the TFPU-bentonite contact surface was established and verified. The influences of normal stress on the damage evolution and the critical damage of the contact surface during the shearing process were analyzed. The shear damage model proposed here can describe the softening characteristic and stress state of the TFPU-bentonite contact surface during shear. This study provides a theoretical base for evaluating the effects of the TFPU-soil contact surface on the mechanical behavior of the TFPU cut-off wall structures in the soil.

2. Materials and Methods

The calcium-based bentonite and TFPU grouting material were used to prepare the tested samples. The bentonite is with a density of 1.61 g/cm^3, the montmorillonite content of 75%, and the moisture content of 22%. The bentonite was compacted layer by layer by impacting and each layer was impacted 30 times with a heavy load to a height half the mold size, followed by grouting with TFPU material to fill the remaining spaces [26]. TFPU is the polymerization reaction product of isocyanate and polyols at a mass ratio of 1 : 1 [15, 26]. The isocyanate and polyols are liquids, and they were firstly atomized into microdrops with the significantly increased specific surface area using the high-pressure nitrogen flow (8.0 MPa), and then the two droplets were simultaneously injected into the closed molds [12, 13, 26]. The polymerization reaction between the raw materials occurs so fast that they cannot be fully mixed with the plain mechanical stirring method [37]. Through the atomization treatment, the well-mixed materials could be obtained [38]. Compared with the compaction load, the expansion force of the TFPU is small [39]; therefore, the grouting process of TFPU brings little influence on the pore structure and moisture content of the bentonite. More details about the fabrication and curing procedures of TFPU-bentonite samples are included in Reference [26].

The prepared samples were cubic with a side length of 100 mm. The moisture content of the bentonite here was the optimum (22%), and the density of the TFPU was 0.488 g/cm^3, the commonly designed density in actual engineering [9, 26]. The density of TFPU was controlled by fixing the injection time at 30 s based on the previous experiences of grouting experiment [12]. Studies on the mechanical properties of the two materials show that bentonite was with the cohesion force of about 123 kPa and friction angle of 19°, respectively, and that the shear strength of the TFPU can be about 4 times that of bentonite under the same normal stress [26].

The direct shear test was conducted on the TFPU-bentonite samples to obtain information about the shear strength of the contact surfaces. Before shearing, the designed normal stress (σ_N) was applied to the samples and it was maintained as constant during shearing. Four σ_N (75, 300, 600, and 1200 kPa) were adopted. The shearing of the contact surfaces was achieved by applying the horizontal displacement to the bentonite part at a rate of 1 mm/min for simulating the static shear load [40]. A DH5902 N data acquisition system was used to record real-time horizontal stress and displacement.

3. Results and Discussion

3.1. Experimental Results. Previous studies on the shear strength of the soil-concrete or soil-rock contact surfaces have pointed out that the shear failure mainly happens in the low-strength medium near the contact surfaces, and the thickness of the shear failure zone is usually about 1/100–1/10 of the contact surface length [41, 42]. Here, the thickness of the shear failure zone was determined as 10 mm, about 1/10 of the length of the contact surfaces, which has also been confirmed by the digital photographic test results [26]. According to this assumption and the shear displacement, γ, the shear strain, can be obtained and the shear stress-

shear strain (τ-γ) curves can be drawn (as shown in Figure 2).

From Figure 2, it can be found that τ increases almost linearly with the increasing γ in Stage I and that the increasing rate of τ declines in Stage II and the plastic deformation occurs. The plastic deformation is caused by the gradual accumulation of the damage on the contact surface [30, 32]. When the accumulated damage reaches its critical value, τ reaches the peak value (the yield point), and after that, with the further increasing γ, τ declines gradually (Stage III), implying the strain-softening phenomenon [29]. Finally, the plateaus can be achieved on the τ-γ curves (Stage IV) and τ_0, and the almost unchanged shear stress in Stage IV is known as the residual strength. Figure 2 also presents that in both G_0, the slope of the τ-γ curves in Stage I, τ_y and γ_y (the shear stress and shear strain at the yield point), and τ_0 increases when σ_N increases and that the strain-softening behavior becomes less significant with the increasing σ_N. G_0 represents the shear modulus of the TFPU-bentonite contact surfaces.

The specific values of parameters G_0, τ_y, γ_y, and τ_0 obtained from Figure 2 are listed in Table 1. The variations of τ_y with σ_N are often linearly fitted, and then the cohesion force (c) and friction angle (φ) of the contact surfaces can be obtained according to the More–Coulomb theory [43]. The calculated c and φ are 174.2 kPa and 40.8°, respectively [26].

Figure 3 shows the variation laws of G_0 and τ_0 with σ_N, from which one can see that the change of G_0 with σ_N confirms the form of the power function. In Figure 3(a), the parameter P_a is introduced to make the expression independent of the choice of the units [44]. The parameter P_a is commonly seen when describing the variation laws of modulus using the mathematical equations and its value is often determined as 101 kPa (1 atm) following the usual suggestion [44]. This power function can simultaneously reflect the effects of both the material properties of the contact surface and the normal stress. Figure 3(b) shows that τ_0 varies linearly with σ_N. This is because the residual strength is mainly provided by interfacial friction that is linearly dependent on normal pressure [45, 46]. The two functions are with a high goodness of fit (with the coefficient of determination of higher than 0.95), indicating that they can describe the variation laws of G_0 and τ_0 with σ_N well.

3.2. The Damage Model of the TFPU-Bentonite Contact Surface. From the macroscopic perspective, the shear failure is caused by the failure of a thin layer of soil near the contact surface [28, 41, 42]. Figure 4 shows the schematic diagram of the failure process of the shear zone [29], where A' and A'' represent the intact area and the damaged area, respectively. The damage of the shear zone, D, can be calculated as the following:

$$D = \frac{A''}{A' + A''}. \tag{1}$$

Due to the existence of normal stress during shearing, the damaged area can bear shear stress through friction as well [45]. Assuming that the shear stress on the intact area and the damaged area is τ' and τ'', respectively, τ, the total shear stress on the shear fracturing plane can be calculated by

$$\tau = \frac{\tau' A' + \tau'' A''}{A' + A''}. \tag{2}$$

Substituting (1) into (2) gives the following equation:

$$\tau = \tau' (1 - D) + \tau'' D. \tag{3}$$

The variation of the shear stress on the intact area with the shear strain can be considered linearly. Therefore, τ' can be calculated as the following:

$$\tau' = G' \cdot \gamma, \tag{4}$$

where G' represents the initial shear modulus of the materials in the intact area. The τ-γ curves presented in Figure 2 show that in Stage I, the shear modulus of the samples is almost the constant, indicating that there exists little damage [30]. Therefore, G' can be represented by G_0.

Based on equations (3) and (4), the following equation can be obtained as follows:

$$\tau = G_0 \cdot (1 - D) \cdot \gamma + \tau'' \cdot D. \tag{5}$$

According to the statistical strength theory [29, 47–49], the distribution of D of the shear zone can be written as the Weibull formula:

$$D = 1 - \exp\left[-\left(\frac{\gamma}{n}\right)^m\right], \tag{6}$$

where m and n are the Weibull parameters.

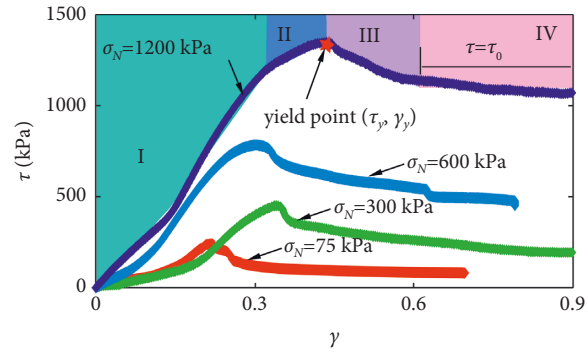

Figure 2: τ-γ curves of the TFPU-bentonite contact surface under different σ_Ns.

Table 1: Mechanical properties of the TFPU-bentonite contact surfaces.

σN (kPa)	G_0 (kPa)	τ_y (kPa)	γ_y	τ_0 (kPa)
75	1012.2	240.33	0.245	97.6
300	1604.4	428.92	0.299	237.4
600	2626.2	784.71	0.353	546.7
1200	3736.4	1349.55	0.431	1135.8

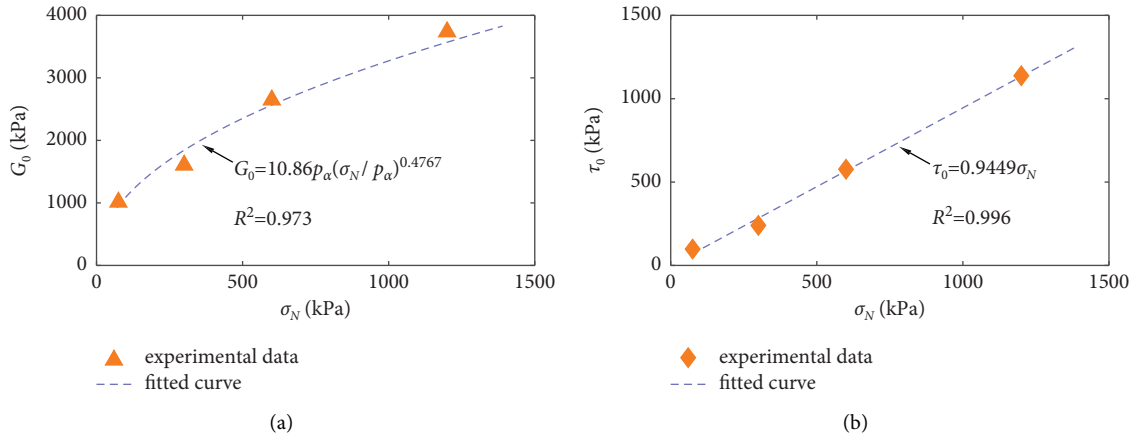

Figure 3: Variations of (a) G_0 and (b) τ_0 with σ_N. (p_a and R^2 representing the reference pressure and the coefficient of determination, respectively).

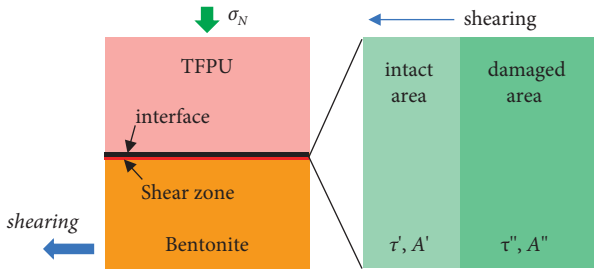

Figure 4: Schematic diagram of the development of the shear damage of the TFPU-bentonite contact surface.

Substituting (6) into (5) gives the shear damage function of the contact surface between TFPU and bentonite:

$$\tau = (G_0 \cdot \gamma - \tau'') \cdot \exp\left[-\left(\frac{\gamma}{n}\right)^m\right] + \tau''. \quad (7)$$

According to (7), the specific form of the damage function of the TFPU-bentonite contact surfaces can be obtained when the specific values of parameters G_0, τ", m, and n are provided. Equation (3) shows that τ equals τ" when D reaches to 1.0, and Figure 2 shows that τ equals τ_0 when the interfaces are completely failed ($D = 1.0$). Therefore, τ" can be represented as the following:

$$\tau'' = \tau_0. \quad (8)$$

The τ-γ curves also tell us that the nominal shear stress reaches its maximum at the yield point. Therefore, equation (7) gives the maximum value of τ when γ equals γ_y, i e., the following equation holds:

$$\frac{d\tau}{d\gamma}\Big|_{\gamma=\gamma_y} = 0. \quad (9)$$

By solving (9), the following equation can be obtained as follows:

$$\frac{G_0 \cdot n}{(G_0 \cdot \gamma_y - \tau_0) \cdot m} = \left(\frac{\gamma_y}{n}\right)^{m-1}. \quad (10)$$

Substituting (10) into (7) gives the following equation:

$$\ln\left(\frac{\tau_y - \tau_0}{G_0 \cdot \gamma_y - \tau_0}\right) = -\frac{G_0 \cdot \gamma_y}{(G_0 \cdot \gamma_y - \tau_0) \cdot m}. \quad (11)$$

where τ_y represents the shear stress when γ reaches γ_y.

Based on (10), the Weibull parameter n can be calculated as the following:

$$\gamma_y \cdot \left[\left(1 - \frac{\tau_0}{G_0 \cdot \gamma_y}\right) \cdot m\right]^{\frac{1}{m}} = n. \quad (12)$$

It can be seen that the specific value of parameter m can be obtained by substituting G_0, τ_y, γ_y, and τ_0 into (11), and then substituting m and other related parameters into (12) can obtain the specific value of parameter n. Table 2 gives the calculated values of parameters m and n, and their variation laws with γ are shown in Figure 5.

Figure 5 shows that with the increasing σ_N, the Weibull parameter m declines, whereas the Weibull parameter n increases gradually. The variation laws of the Weibull parameters with σ_N conform to the form of the power function. The coefficients of determination R^2 of the functions presented in Figure 5 are higher than 0.95, indicating the enough-high goodness of fit. Substituting the functions presented in Figure 3, Figure 5, equation (8) into equation (7) gives the specific form of the shear softening damage function that contains two independent variables: σ_N and γ, i.e., $\tau = f(\sigma_N, \gamma)$.

3.3. Verification of the Damage Model. The damage equation established in Section 3.2 can theoretically describe the variations of τ with γ during shearing. But it is necessary to evaluate its reasonableness. Figure 6 shows the comparison between the experimental and theoretical τ-γ curves of TFPU-bentonite contact surfaces under different normal stress, and the probability distribution of differences in the experimental and theoretical data is presented in Figure S1.

Table 2: The calculated values of the Weibull parameters m and n.

σ_N (kPa)	75	300	600	1200
m	31.545	8.238	4.801	4.226
n	0.269	0.356	0.401	0.454

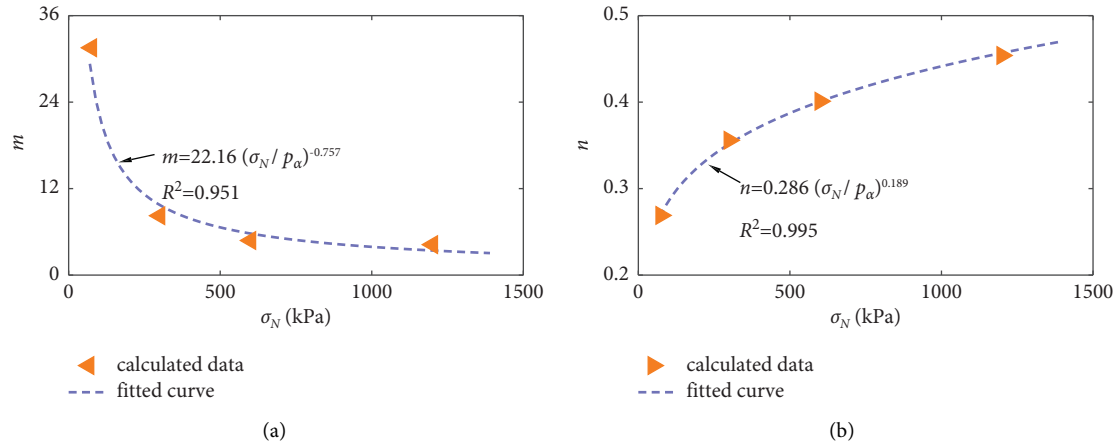

Figure 5: Variations of the Weibull parameters (m) and (n) with σ_N. (p_a and R^2 represent the reference pressure and the coefficient of determination, respectively).

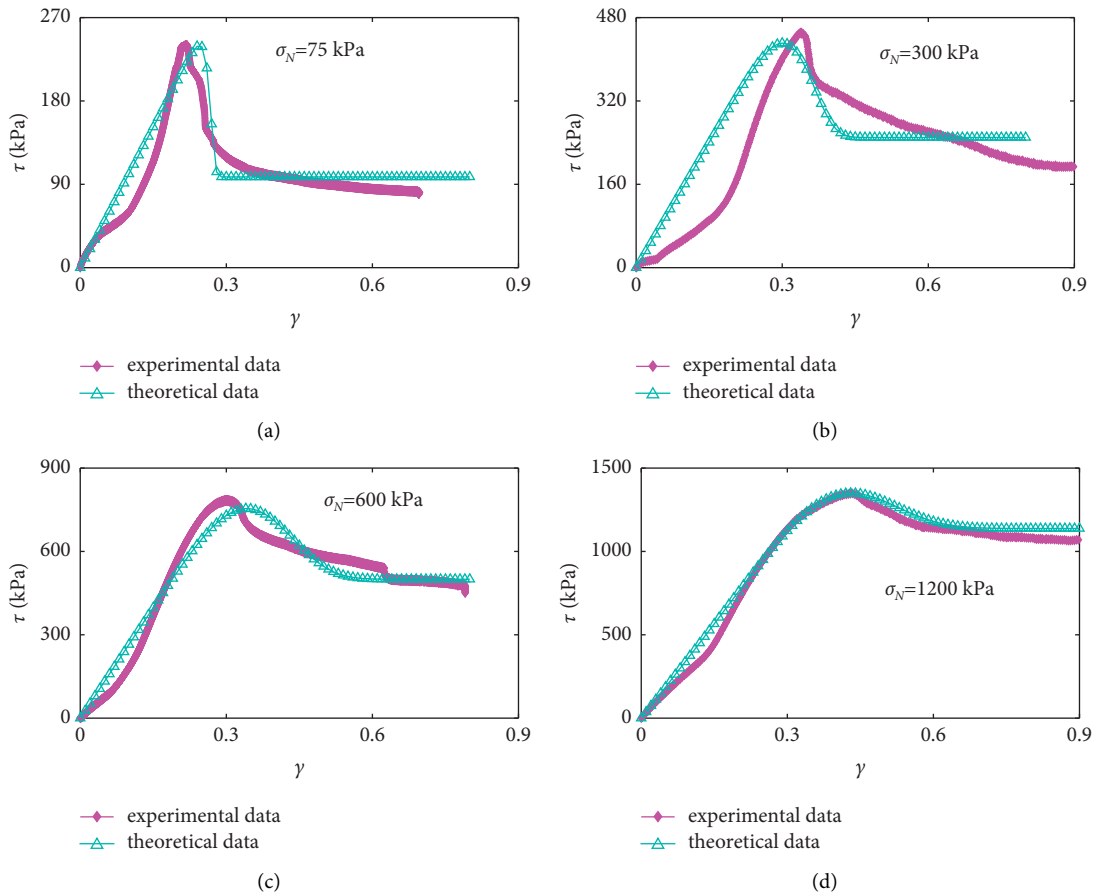

Figure 6: Comparison between the experimental and theoretical τ-γ curves of the TFPU-bentonite contact surface under different σ_N.

Table 3: The theoretical shear stress and shear strain of the contact surfaces at the yield point.

σ_N (kPa)	75	300	600	1200
τ_y (kPa)	240.31	431.11	754.26	1348.56
γ_y	0.241	0.301	0.341	0.423

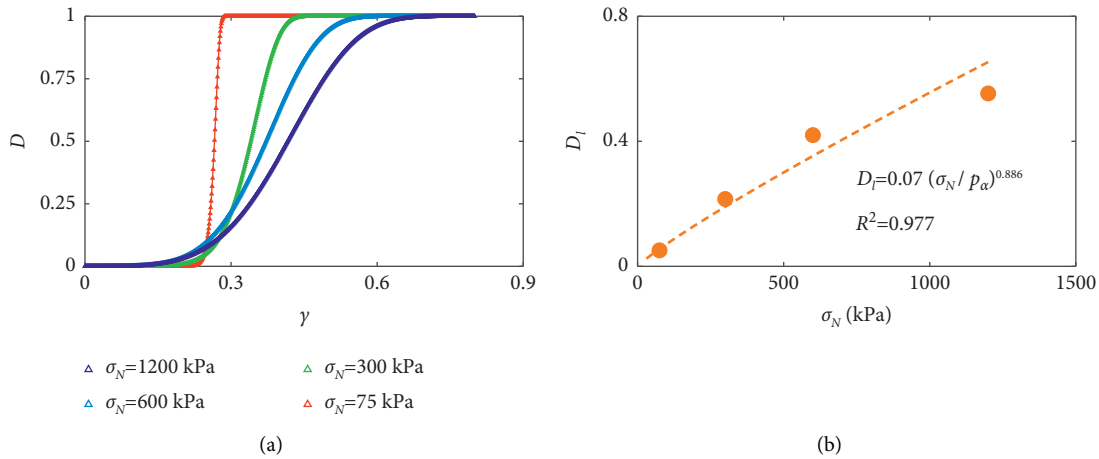

Figure 7: Variations of (a) D versus γ and (b) D_l versus σ_N. D_l is the critical damage. p_a was introduced to make the expression independent of the choice of the units, and its value is 101 kPa [44].

The theoretical τ and γ at the yield point are calculated and they are listed in Table 3.

Figure 6 tells us that even though these exist some differences, the theoretical τ-γ curves can reflect the primary variation characteristics of τ with γ. Both the linear growth state, yield stage, strain-softening behavior, and the residual strength can be seen on the theoretical τ-γ curves. It can also be found from Figure 6 and Figure S1 that with the increasing σ_N, the coincidence degree of the theoretical and experimental curves becomes higher and higher and that the two curves almost overlap at σ_N of 1200 kPa. Figure S1 shows that the relative difference between over 80% experimental and theoretical τ is lower than 30%. Moreover, compared with the experimental data (Table 1), the maximum relative errors of τ_y and γ_y are around 3.88% and 3.40% (at σ_N of 600 kPa), respectively. These differences are acceptable from the actual engineering perspective [50]. Therefore, the shear damage function proposed here can be used to describe the variation of shear stress on the contact surfaces between the TFPU matrix and bentonite.

Figure 7 presents the evolution process of damage during shearing and the variations of the critical damage (D_l) with σ_N. D_l is derived from equation (7), and it represents the damage when the shear stress of the contact surface reaches the yield strength. The variation curves of D are drawn based on equation (6), and D_l was calculated by (13). From Figure 7, one can see that D remains zero until γ reaches a certain value, after which, it increases with the increasing γ until up to 1. This observation corresponds well with the characteristics of the experimentally obtained τ-γ curves (Figure 2). When σ_N increases from 75 to 1200 kPa, the rate at which D increases with the increasing γ, whereas D_l of the TFPU-bentonite contact surface increases in the power function way and they are within the range of about 0.05 ~ 0.50 (Figure 7(b)). The observations on the evolution of D and the variation laws of D_l indicate that with the increasing normal stress, the shear failure of the TFPU-bentonite contact surface changes from brittleness to ductility. Here, bentonite was used because it is commonly seen in the TFPU cut-off wall engineering [26]. The mechanical properties between bentonite and other types of soil, such as the sand soil, are different [51]; therefore, the shear damage model established here may not be applicable to the contact surfaces between TFPU and other types of soil, but this study highlights the idea of proposing theoretical damage model for the commonly seen contact surfaces.

$$D_l = \frac{G_0 \cdot \gamma_y - \tau_y}{G_0 \cdot \gamma_y - \tau_0}. \tag{13}$$

4. Conclusions

In this study, the shear strength of the TFPU-bentonite contact surface under different normal stress was experimentally measured and the corresponding shear damage model was established and verified. The following conclusions are drawn:

(1) Under shear, the stress-strain curves of the TFPU-bentonite contact surface contain the linear increasing segment, the yield segment, the strain-softening segment, and the residual strength segment. With the increasing normal stress, the shear

modulus and residual strength of the contact surface increase in the power function and linear function way, respectively, whereas the strain-softening phenomenon is less and less obvious.

(2) The theoretical shear stress-strain curves have high goodness of fit with those obtained through the direct shear test, and the maximum differences in the theoretical and experimental yield shear stress and yield shear strain are separately about 3.88% and 3.40%. The established shear softening damage model can reflect the strain-softening characteristic and the stress state of the TFPU-bentonite contact surface.

(3) The theoretical variation laws of D versus γ correspond well with the characteristics of the experiment τ-γ curves. With the increased normal stress on the TFPU-bentonite contact surface, the rate at which D increases with the increasing γ declines, whereas the critical damage increases in the power function way (within 0.05 ~ 0.50) and the shear failure of the TFPU-bentonite contact surfaces changes from brittleness to ductility.

Data Availability

The data used to support the findings of the study are available from the corresponding author upon request.

Conflicts of Interest

The authors declare that they have no conflicts of interest.

Acknowledgments

The authors are grateful for the financial support from the National Natural Science Foundation of China (Grant no. 51908515).

Supplementary Materials

Figure S1 shows the probability distribution of differences in the experimental and theoretical t-γ curves of TFPU-bentonite contact surfaces under different normal stress. In Figure S1, R_a represents the relative error between the experimental and theoretical data of τ at different γ, and P_d and C_p represent the probability density and the cumulative probability density of R_a. (*Supplementary Materials*)

References

[1] L. Lam, D. G. Fredlund, and S. L. Barbour, "Transient seepage model for saturated-unsaturated soil systems: a geotechnical engineering approach," *Canadian Geotechnical Journal*, vol. 24, no. 4, pp. 565–580, 1987.

[2] B. Li, F. Wang, H. Fang, K. Yang, X. Zhang, and Y. Ji, "Experimental and numerical study on polymer grouting pretreatment technology in void and corroded concrete pipes," *Tunnelling and Underground Space Technology*, vol. 113, no. 3, Article ID 103842, 2021.

[3] X. Cai, Z. Zhou, H. Zang, and Z. Song, "Water saturation effects on dynamic behavior and microstructure damage of sandstone: phenomena and mechanisms," *Engineering Geology*, vol. 276, p. 105760, 2020.

[4] X. Cai, Z. Zhou, and X. Du, "Water-induced variations in dynamic behavior and failure characteristics of sandstone subjected to simulated geo-stress," *International Journal of Rock Mechanics and Mining Sciences*, vol. 130, Article ID 104339, 2020.

[5] X. Cai, C. Cheng, Z. Zhou, H. Konietzky, Z. Song, and S. Wang, "Rock mass watering for rock-burst prevention: some thoughts on the mechanisms deduced from laboratory results," *Bulletin of Engineering Geology and the Environment*, vol. 80, no. 11, pp. 8725–8743, 2021.

[6] S. Hinchberger, J. Weck, and T. Newson, "Mechanical and hydraulic characterization of plastic concrete for seepage cut-off walls," *Canadian Geotechnical Journal*, vol. 47, no. 4, pp. 461–471, 2010.

[7] A. R. Bagheri, M. Alibabaie, and M. Babaie, "Reduction in the permeability of plastic concrete for cut-off walls through utilization of silica fume," *Construction and Building Materials*, vol. 22, no. 6, pp. 1247–1252, 2008.

[8] W. Schönfelder, J. Dietrich, A. Märten, K. Kopinga, and F. Stallmach, "NMR studies of pore formation and water diffusion in self-hardening cut-off wall materials," *Cement and Concrete Research*, vol. 37, no. 6, pp. 902–908, 2007.

[9] F. Wang, J. Li, M. Shi, and C. Guo, "New seepage-proof and reinforcing technologies for dikes and dams and their applications," *Journal of Hydroelectric Engineering*, vol. 35, no. 12, pp. 1–11, 2016.

[10] S. Zhang, B. Xue, J. Wang, J. Gao, C. Wang, and W. Li, "Preliminary study of nondestructive testing of the polymer cutoff wall based on vibration theory," *Advances in Materials Science and Engineering*, vol. 2021, Article ID 4444684, 2021.

[11] A. N. Antão, N. M. D. C. Guerra, M. Matos Fernandes, and A. S. Cardoso, "Influence of tension cut-off on the stability of anchored concrete soldier-pile walls in clay," *Canadian Geotechnical Journal*, vol. 45, no. 7, pp. 1036–1044, 2008.

[12] M. Li, M. Du, F. Wang, B. Xue, C. Zhang, and H. Fang, "Study on the mechanical properties of polyurethane (PU) grouting material of different geometric sizes under uniaxial compression," *Construction and Building Materials*, vol. 259, Article ID 119797, 2020.

[13] Z. Wang, M. Du, H. Fang, C. Zhang, M. Li, and M. Shi, "Influence of different corrosion environments on mechanical properties of a roadbed rehabilitation polyurethane grouting material under uniaxial compression," *Construction and Building Materials*, vol. 301, Article ID 124092, 2021.

[14] X. Lou, R. Wang, and Y. Zhou, "Polymer cut-off wall quality testing based on direct current response measuring," *Advanced Materials Research*, vol. 838-841, pp. 1715–1718, 2013.

[15] F. M. Wang, M. S. Shi, H. J. Li, and Y. H. Zhong, "Experimental study on the anti-permeability properties of polymer grouting materials," *Advanced Materials Research*, vol. 284-286, pp. 1952–1955, 2011.

[16] Q. Ma and M. Zhu, "Discussion on a new technique for controlling the seepage damage to an ancient tomb," *Electronic Journal of Geotechnical Engineering*, vol. 21, pp. 5319–5328, 2016.

[17] J. Schwarzbauer, S. Heim, S. Brinker, and R. Littke, "Occurrence and alteration of organic contaminants in seepage and leakage water from a waste deposit landfill," *Water Research*, vol. 36, no. 9, pp. 2275–2287, 2002.

[18] C. Yu, S. C. Deng, H. B. Li, J. C. Li, and X. Xia, "The anisotropic seepage analysis of water-sealed underground oil storage caverns," *Tunnelling and Underground Space Technology*, vol. 38, pp. 26–37, 2013.

[19] J. Xu, F. M. Wang, Y. Zhong, B. Wang, X. Li, and N. Sun, "Stress analysis of polymer diaphragm wall for earth-rock dams under static and dynamic loads," *Chinese Journal of Geotechnical Engineering*, vol. 34, no. 9, pp. 1699–1704, 2012.

[20] F. Wang, J. Xu, L. Yang, Y. Zhong, and J. Li, "Static load experiment and numerical analysis of polymer diaphragm wall of dam," *Journal of Architecture and Civil Engineering*, vol. 32, no. 2, pp. 27–34, 2015.

[21] J. Li, J. Zhang, and B. Wang, "Research on multiple-objective function optimization method for polymer anti-seepage wall under seismic loads," *World Earthquake Engineering*, vol. 33, no. 4, pp. 106–113, 2017.

[22] J. Liu, D. Chang, and Q. Yu, "Influence of freeze-thaw cycles on mechanical properties of a silty sand," *Engineering Geology*, vol. 210, pp. 23–32, 2016.

[23] M. Cao, C. Wang, R. Xia et al., "Preparation and performance of the modified high-strength/high-modulus polyvinyl alcohol fiber/polyurethane grouting materials," *Construction and Building Materials*, vol. 168, no. 20, pp. 482–489, 2018.

[24] L. Pietola, R. Horn, and M. Yli-Halla, "Effects of trampling by cattle on the hydraulic and mechanical properties of soil," *Soil and Tillage Research*, vol. 82, no. 1, pp. 99–108, 2005.

[25] A. Haraldsson and P. Wriggers, "A strategy for numerical testing of frictional laws with application to contact between soil and concrete," *Computer Methods in Applied Mechanics and Engineering*, vol. 190, no. 8-10, pp. 963–977, 2000.

[26] M. Li, H. Fang, M. Du, C. Zhang, Z. Su, and F. Wang, "The behavior of polymer-bentonite interface under shear stress," *Construction and Building Materials*, vol. 248, Article ID 118680, 2020.

[27] G. Zhang and J. Zhang, "Unified modeling of soilstructure interface and its test confirmation," *Chinese Journal of Geotechnical Engineering*, vol. 27, no. 10, pp. 1175–1179, 2005.

[28] Y. Long, J. Zhang, and J. Chen, "Study on shear damage model for soil-structure interface based on Weibull distribution," *Journal of Highway and Transportation Research and Development*, vol. 34, no. 5, pp. 65–71, 2017.

[29] Y. Long, J. Zhang, and J. Chen, "Shear characteristics of structure interface and its strain-softening and hardening damage model," *Journal of South China University of Technology*, vol. 44, no. 12, pp. 128–134, 2016.

[30] A. D. Jefferson, "Craft--a plastic-damage-contact model for concrete. I. Model theory and thermodynamic considerations," *International Journal of Solids and Structures*, vol. 40, no. 22, pp. 5973–5999, 2003.

[31] Z. Song, H. Konietzky, and X. Cai, "Modulus degradation of concrete exposed to compressive fatigue loading: insights from lab testing," *Structural Engineering & Mechanics*, vol. 78, no. 3, pp. 281–296, 2021.

[32] N. Wechsler, T. K. Rockwell, and Y. Ben-Zion, "Application of high resolution DEM data to detect rock damage from geomorphic signals along the central San Jacinto Fault," *Geomorphology*, vol. 113, no. 1-2, pp. 82–96, 2009.

[33] T. Zhu, J. Chen, D. Huang et al., "A DEM-based approach for modeling the damage of rock under freeze-thaw cycles," *Rock Mechanics and Rock Engineering*, vol. 54, no. 6, pp. 2843–2858, 2021.

[34] L. Yu, A. Fu, Q. Yin, H. Jing, T. Zhang, and H. Qin, "Dynamic fracturing properties of marble after being subjected to multiple impact loadings," *Engineering Fracture Mechanics*, vol. 230, Article ID 106988, 2020.

[35] Y. Lai, L. Jin, and X. Chang, "Yield criterion and elasto-plastic damage constitutive model for frozen sandy soil," *International Journal of Plasticity*, vol. 25, no. 6, pp. 1177–1205, 2009.

[36] Y. Long, J.-H. Chen, and J.-S. Zhang, "Introduction and analysis of a strain-softening damage model for soil-structure interfaces considering shear thickness," *Ksce Journal of Civil Engineering*, vol. 21, no. 7, pp. 2634–2640, 2017.

[37] F. Wang, C. Guo, and Y. Gao, "formation of a polymer thin wall using the level set method," *International Journal of Geomechanics*, vol. 14, no. 5, Article ID 04014021, 2014.

[38] X. Li and M. C. Soteriou, "High fidelity simulation and analysis of liquid jet atomization in a gaseous crossflow at intermediate Weber numbers," *Physics of Fluids*, vol. 28, no. 8, Article ID 082101, 2016.

[39] X. Du, H. Fang, S. Wang, B. Xue, and F. Wang, "Experimental and practical investigation of the sealing efficiency of cement grouting in tortuous fractures with flowing water," *Tunnelling and Underground Space Technology*, vol. 108, Article ID 103693, 2021.

[40] S. Ouellet, D. Cronin, and M. Worswick, "Compressive response of polymeric foams under quasi-static, medium and high strain rate conditions," *Polymer Testing*, vol. 25, no. 6, pp. 731–743, 2006.

[41] C. S. Desai, M. M. Zaman, J. G. Lightner, and H. J. Siriwardane, "Thin-layer element for interfaces and joints," *International Journal for Numerical and Analytical Methods in Geomechanics*, vol. 8, no. 1, pp. 19–43, 2010.

[42] Z. Yin, H. Zhu, and G. Xu, "Numerical simulation of the deformation in the interface between soil and structural material," *Chinese Journal of Geotechnical Engineering*, vol. 16, no. 3, pp. 14–22, 1994.

[43] J. Escartín, G. Hirth, and B. Evans, "Nondilatant brittle deformation of serpentinites: implications for Mohr-Coulomb theory and the strength of faults," *Journal of Geophysical Research: Solid Earth*, vol. 102, no. 2, pp. 2897–2914, 1997.

[44] S. Rampello, G. M. B. Viggiani, and A. Amorosi, "Small-strain stiffness of reconstituted clay compressed along constant triaxial effective stress ratio paths," *Géotechnique*, vol. 47, no. 3, pp. 475–489, 1997.

[45] C. Di Maio, G. Scaringi, and R. Vassallo, "Residual strength and creep behaviour on the slip surface of specimens of a landslide in marine origin clay shales: influence of pore fluid composition," *Landslides*, vol. 12, no. 4, pp. 657–667, 2015.

[46] H. Yoshizawa, Y. L. Chen, and J. Israelachvili, "Fundamental mechanisms of interfacial friction. 1. Relation between adhesion and friction," *Journal of Physical Chemistry*, vol. 97, no. 16, pp. 4128–4140, 1993.

[47] H. Xie and F. Gao, "The mechanics of cracks and a statistical strength theory for rocks," *International Journal of Rock Mechanics and Mining Sciences*, vol. 37, no. 3, pp. 477–488, 2000.

[48] J. Geng and L. Cao, "Failure analysis of water-bearing sandstone using acoustic emission and energy dissipation," *Engineering Fracture Mechanics*, vol. 231, Article ID 107021, 2020.

[49] X. Li, K. Peng, J. Peng, and D. Hou, "Effect of thermal damage on mechanical behavior of a fine-grained sandstone," *Arabian Journal of Geosciences*, vol. 14, no. 13, p. 1212, 2021.

[50] T. Hanai, T. Ohki, H. Honda, and T. Kobayashi, "Analysis of initial conditions for polymerization reaction using fuzzy neural network and genetic algorithm," *Computers & Chemical Engineering*, vol. 27, no. 7, pp. 1011–1019, 2003.

[51] Y. A. Rogatin and Y. N. Galin, "Mechanical properties of sandy soil at different depths," *Soil Mechanics and Foundation Engineering*, vol. 12, no. 1, pp. 46–49, 1975.